Myosin XI-i Links the Nuclear Membrane to the Cytoskeleton to Control Nuclear Movement and Shape in *Arabidopsis*

Kentaro Tamura,[1] Kosei Iwabuchi,[1] Yoichiro Fukao,[2] Maki Kondo,[3] Keishi Okamoto,[1] Haruko Ueda,[1] Mikio Nishimura,[3] and Ikuko Hara-Nishimura[1,*]

[1]Department of Botany, Graduate School of Science, Kyoto University, Kyoto 606-8502, Japan.

[2]Graduate School of Biological Sciences, Nara Institute of Science and Technology, Ikoma 630-0101, Japan.

[3]Department of Cell Biology, National Institute for Basic Biology, Okazaki 444-8585, Japan.

Running head: Myosin XI-i on the Plant Nuclear Envelope

[*]Correspondence: ihnishi@gr.bot.kyoto-u.ac.jp (I. H-N.)

Summary

The cell nucleus communicates with the cytoplasm through a nucleocytoplasmic linker, which maintains the shape of the nucleus and mediates its migration. In contrast to animal nuclei that are moved by motor proteins (kinesins and dyneins) along the microtubule cytoskeleton [1, 2], plant nuclei move rapidly and farther along an actin filament cytoskeleton [3]. This implies that plants use a distinct nucleocytoplasmic linker for nuclear dynamics, although its molecular identity is unknown. Here, we describe a new type of nucleocytoplasmic linker consisting of a myosin motor and nuclear membrane proteins. In the *Arabidopsis thaliana* mutant *kaku1*, nuclear movement was impaired and the nuclear envelope was abnormally invaginated. The responsible gene was identified as *myosin XI-i*, which encodes a plant-specific myosin. Myosin XI-i is specifically localized on the nuclear membrane where it physically interacts with the outer-nuclear membrane proteins WIT1 and WIT2. Both WIT proteins are required for anchoring myosin XI-i to the nuclear membrane and for nuclear movement. A striking feature of plant cells is dark-induced nuclear positioning in mesophyll cells. A deficiency of either myosin XI-i or WIT proteins diminished dark-induced nuclear positioning. The unique nucleocytoplasmic linkage in plants might enable rapid nuclear positioning in response to environmental stimuli.

Results and Discussion

In plant cells, nuclei move large distances along the actin filaments, often undergoing shape changes as they move [3]. They move more rapidly than animal nuclei by an unknown mechanism that does not involve microtubules. To identify this mechanism, we used a forward genetics approach. A transgenic *Arabidopsis thaliana* plant that expressed the nuclear marker Nup50a-GFP [4] had spindle-shaped nuclei in the epidermal cells of leaves (Figure 1A) and other tissues including root hairs, root cells, and hypocotyls (see Figure S1A available online). From an ethyl methanesulfonate-mutagenized population of the transgenic plant, a mutant with abnormal nuclear shapes and a defect in nuclear movement was isolated and designated as *kaku1-1*, after the Japanese word for nucleus. The *kaku1-1* nuclei were nearly spherical in various tissues (Figure 1B; Figure S1A), with a significantly higher circularity index [4π (area/perimeter^2)] than wild-type nuclei (Figure S1B). The circularity index decreased with increasing nuclear size in wild-type cells, but not in *kaku1-1* cells (Figure S1C). To visualize the nuclear envelope, an RFP fusion protein with the inner membrane protein SUN2 [5-7] was stably expressed in wild-type and *kaku1-1* plants. The wild-type nuclear envelope was elongated along the longitudinal axis of the root hair cell (Figure 1C). By contrast, the *kaku1-1* envelope was irregularly and intricately invaginated (Figure 1D). Electron micrographs showed that the nuclear envelope was deeply invaginated in *kaku1-1* (Figure 1F; Figure S1D), but not in the wild type (Figure 1E). These results suggest that the *KAKU1* plays an important role in nuclear envelope shape.

The *kaku1-1* mutant had a point mutation at the splice donor site of the third intron of the At4g33200 gene (Figure 1G) and lacked any detectable At4g33200 transcripts (Figure 1H), suggesting that *kaku1-1* is a null mutant. All of three T-DNA tagged alleles (*kaku1-2*, *kaku1-3*, and *kaku1-4*) (Figure 1G), which were also null mutants (Figure 1H), had spherical nuclei like those of *kaku1-1* (Figure 1I), indicating that the At4g33200 gene is responsible for the *kaku1* phenotype. The *KAKU1* gene

encodes a plant-specific myosin (173 kDa) that belongs to the myosin XI family. *A. thaliana* has 13 members in the myosin XI family: myosins XI-a to XI-k and myosins XI-1 (Mya1) and XI-2 (Mya2) [8]. KAKU1 clustered with myosin XI-i subfamily proteins, which are conserved widely in land plants [8-10]. Of all the single mutants of the 13 members, only *myosin xi-i/kaku1* exhibited abnormal nuclear shape (Figure S1E), indicating that myosin XI-i is the predominant myosin XI involved in elongated shapes of nuclei.

Myosin XI family proteins have a highly conserved motor domain, six IQ motifs, a coiled coil responsible for dimerization, and a tail domain involved in targeting [11]. We generated a transgenic plant expressing a YFP conjugated with myosin XI-i lacking the motor domain (YFP-XI-i-Δmotor), in which the transgene level was estimated to be 11.48 ± 0.80 times the endogenous *myosin XI-i/KAKU1* gene level by quantitative RT-PCR (data not shown). In the transgenic plants, nuclear morphology was indistinguishable from that in the wild type, suggesting that expression of the transgene had no dominant negative effect on nuclear morphology. The fusion protein from the transgenic plants gave a single band with a molecular mass of 105 kDa corresponding to the full-length fusion protein, but no degradation products on the immunoblot with anti-GFP antibody (Figure 1J). The fluorescent signal of YFP-XI-i-Δmotor was clearly visible on the nuclear membrane in epidermal cells of cotyledons and roots (Figure 1K), in agreement with a previous report [12]. Furthermore, full-length myosin XI-i fused with GFP also localized on the nuclear membrane in protoplasts from cultured tobacco cells (Figure 1L). These results suggested that myosin XI-i localized to the nuclear membrane.

To clarify whether myosin XI-i functions in nuclear movement, a GFP-tagged histone was stably expressed in each of the *kaku1-2* and *kaku1-4* mutants and the wild type. Nuclear movement in the root cells of seedlings was examined by imaging the fluorescent nuclei of three-dimensional reconstitutions for 45 min. In wild-type cells, the spindle-shaped nuclei moved rapidly and bidirectionally for a distance equal

to the whole cell length (Figure 1M; Movie S1). By contrast, in the *kaku1-2* and *kaku1-4* mutants, the spherical nuclei moved much more slowly (Figure 1M; Movie S1). These results suggest that myosin XI-i drives nuclear movement along actin filaments. Such movement is consistent with the finding that actin-depolymerizing drugs abolished nuclear movement in plants [3]. On the other hand, in growing pollen tubes, the *kaku1-4* nuclei moved normally (Figure S1F), which is consistent with normal fertility of all four *kaku1* mutants.

We previously reported that other myosin XI family members, myosin XI-k and XI-2, drive streaming of endoplasmic reticulum (ER) in petiole cells [13]. These myosins regulate the organization of ER network and actin filament [13] (Figures S2C and S2G). However, *kaku1* exhibited no abnormalities in the ER of petiole cells (Figures S2A, S2B and S2D) or in the cortical actin network of hypocotyl cells (Figures S2E, S2F, and S2H), suggesting that myosin XI-i is not directly involved in the ER architecture or the organization of cortical actin filaments. A deficiency of either myosin XI-k or XI-2 in trichome cells results in the appearance of more elongated nuclei [14]. Myosin XI-k and XI-2 might regulate nuclear shapes by different mechanisms from myosin XI-i, because they function in actin organization [13], while myosin XI-i does not (Figures S2E-S2H).

Next, we examined the interactome of transgenic plants expressing YFP-XI-i-Δmotor. The anti-GFP antibody pull-down fraction produced a 105-kDa single band on the immunoblot with anti-GFP antibody, indicating the presence of an intact YFP-XI-i-Δmotor in the fraction (Figure 2A). Mass spectrometry of the immunoprecipitates (Figure S3A) identified WPP domain-interacting tail-anchored protein 2 (WIT2, 72 kDa), which was found in the pull-down fraction from the transgenic plants, but not from the control transgenic plants (Figure S3B). WIT proteins are integral membrane proteins on the outer nuclear membrane. This implies that myosin XI-i is associated with WIT proteins on the outer nuclear membrane (see Figure 4A, discussed below).

A. thaliana has two *WIT* genes, *WIT1* (At5g11390) and *WIT2* (At1g68910), which function redundantly in RanGAP anchoring on the nucleus [15]. Intriguingly, the fluorescent signal of YFP-XI-i-∆motor was no longer detected on the nuclear membranes of either hypocotyl or root epidermal cells in *wit1 wit2* (Figure 2B; Figure S3C), although the expression level of the YFP-XI-i-∆motor fusion protein in *wit1 wit2* was the same as in the wild type (Figure 2C). These results indicate that myosin XI-i had no ability to associate with the nuclear membrane in the absence of WIT proteins. Hence, WIT proteins are required for anchoring myosin XI-i to the nuclear membrane.

A deficiency of both WIT1 and WIT2 caused the nuclei to have abnormal phenotypes similar to the phenotypes caused by a deficiency of myosin XI-i. The nuclear morphological phenotype in root cells was more spherical in the *wit1 wit2* double-mutant than in the wild type and the single-mutants (*wit1* and *wit2*) (Figures 2D and 2E). In root cells of *wit1 wit2* seedlings, nuclear movement was impaired (Figure 2F; Movie S1), as were in the *kaku1-2* and *kaku1-4* (Figure 1M). The nuclear movement rates in root hair cells were 0.52 ± 0.35 μm/min for *kaku1-2*, 0.85 ± 0.46 μm/min for *kaku1-4*, and 0.85 ± 0.70 μm/min for *wit1 wit2*, while the wild type rate was 2.68 ± 1.37 μm/min. A deficiency of either myosin XI-i or WIT proteins caused a significant reduction of the nuclear movement rates (Figure 2G), suggesting that myosin XI-i, which is bound to the outer nuclear membrane through WIT proteins, drives nuclear movement. The myosin XI-i-dependent movement of nuclei was significantly slower than the myosin XI-k-dependent movement of ER in petiole cells (~3.5 μm/sec) [13]. This could be because myosin XI-i has lower motor activity than myosin XI-k. Another possibility is that nuclei are particularly difficult to transport because of their larger size.

A striking feature of plant cells is the movement of nuclei in a light- and dark-dependent manner [16]. In response to strong light, nuclei of leaves move to the anticlinal wall of the cells, which is regulated by the blue-light receptor phototropin2 and the actin filaments [17]. On the other hand, during dark adaptation, nuclei move to

the center of the periclinal wall of the cells to keep away from the plant body surface, which might enable the nucleus to protect from external stresses. However, the molecular mechanism underlying dark-induced nuclear movement is currently unknown. Three-dimensional images of dark-induced nuclear positioning in mesophyll cells were obtained (Movie S2). The majority of the wild-type nuclei were localized together with chloroplasts at the center of the periclinal wall (bottom) of the cells, while hardly any nuclei were located at the anticlinal wall (Figure 3A). By contrast, some nuclei of the *kaku1* and *wit1 wit2* mutants remained at the anticlinal wall, but not at the center of the periclinal (bottom) of the cells (Figure 3A, arrows).

The percentage of nuclei at the anticlinal wall in wild-type leaves, which was approximately 15% in the dark, started to increase immediately in response to blue light irradiation and reached approximately 75% after 3 h irradiation (Figure 3B). The light-induced nuclear movement occurred normally in the *kaku1* and *wit1 wit2* mutants (Figure 3B), suggesting that the myosin XI-i-WIT complex is not involved in light-induced movement. By contrast, during dark adaptation after 3 h of blue-light irradiation, in the *kaku1-2*, *kaku1-4*, and *wit1 wit2* mutants, the relocation of nuclei to the center of the periclinal wall was impaired (Figure 3B). These results indicate that the myosin XI-i-WIT complex plays a role in dark-induced nuclear movement and positioning in mesophyll cells. The fact that the nuclei positioning was not significantly different between the wild type and *wit1 wit2* at 4 h suggested that one or more other factors are also involved in dark-induced nuclear movement.

The question raised is whether myosin XI-i directly interacts with WIT1. A pull-down assay using bacterially expressed recombinant proteins revealed that myosin XI-i-Δmotor specifically and directly bound WIT1 (Figure 4A). Furthermore, the *in vivo* interaction between myosin XI-i and WIT1 was demonstrated by coimmunoprecipitation experiments with tobacco leaves transiently coexpressing YFP-XI-i-Δmotor and RFP-WIT1 (Figure 4B). These results indicate that myosin XI-i directly associates with WIT1 on the nuclear membrane, as shown in the model in

Figure 4C.

Figure 4 (C-E) compares models of the nucleocytoplasmic linkers of plants and animals. In animals, the nucleus communicates with the cytoplasmic microtubules (Figure 4D) or actin filaments (Figure 4E) through (1) an outer-nuclear membrane protein (KASH; Klarsicht/ANC-1/Syne homology) and (2) an inner-nuclear membrane protein (SUN) that interacts with the nuclear lamina [1, 18]. KASH physically interacts with SUN to form the SUN-KASH bridge. The plant counterpart of the SUN-KASH bridge is the SUN-WIP (WPP domain-interacting protein) bridge [19]. As reported [19], WIP1 coimmunoprecipitated with SUN2, although WIP1 lacking a VVPT motif essential for interacting with the SUN domain did not (Figure 4B). WIT [15] and WIP [20], which have no sequence similarities to animal KASH proteins, are tail-anchored proteins on the outer nuclear membrane of plants. WIT1 coimmunoprecipitated with WIP1 (Figure 4B). These results suggest that the WIT-WIP complex in plants can be functionally equivalent to KASH in animals. Myosin XI-i-Δmotor did not coimmunoprecipitate with WIP1 (Figure 4B), which is consistent with the mass spectrometry data (Figure S3B), possibly due to the difficulty of detecting an indirect interaction between the two proteins. Taken together, our results suggest that myosin XI-i interacts with the nucleoplasm through the SUN-WIP-WIT bridge. Here, we describe a new type of nucleocytoplasmic linker involving a myosin motor (myosin XI-i) that binds to both the actin filament cytoskeleton and outer nuclear membrane proteins. To our knowledge, nucleocytoplasmic linkers consisting of a myosin motor have not been reported previously.

Movement, positioning, and anchoring of nuclei, which occur in various cellular processes, are mediated by a linkage between the nucleoplasm and the cytoplasm [1, 18, 21]. Actin filaments are used for nuclear anchoring in mammals [22] and *C. elegans* [23] (Figure 4E). However, no actin-associated motor molecules have been identified in the migration of nuclei in animal cells, although the pushing forces of actin filaments have been implicated in nuclear migration [24, 25]. Animal cells lack long

actin cables with uniform polarity [26, 27]. Therefore, whether myosins are involved in long-distance transport along actin filaments remains controversial [28]. By contrast, in plants, the actin filaments are organized into long bundle structures that are oriented along the longitudinal axes of cells. These actin bundles help to movement of various organelles in plants [13, 29]. Notably, the plant-specific myosin XI family members, which are conserved widely in land plants [8-10], generate high motive forces [30]. Together, these results suggest that plants have evolved a unique machinery involving actin and a myosin motor that enables rapid and long-distance nuclear movement and nuclear positioning in response to environmental stimuli.

Accession Numbers

Sequence data from this article can be found in the GenBank/EMBL data libraries under the accession numbers as follows: Myosin XI-i/KAKU1, At4g33200; SUN1, At5g04990; SUN2, At3g10730; WIP1, At5g26455; WIP2, At5g56210; WIP3, At3g13360; WIT1, At5g11390; WIT2, At1g68910.

Supplemental Information

Supplemental Information includes 4 figures, Supplemental Experimental Procedures, and 2 movies and can be found with this article online at http://www.cell.com/current-biology/supplemental/.

Acknowledgments

We are grateful to Iris Meier (Ohio State University, USA) for a critical reading of the manuscript and for her kind donation of the seeds of *wit1-1*, *wit2-1*, and *wit1-1 wit2*-1 seeds. We are also grateful to Maureen Hanson (Cornell University, USA) for her donation of the YFP-XI-i-∆motor vectors; to Tsuyoshi Nakagawa (Shimane University, Japan) for his donation of the Gateway vectors (pGWB405 and pGWB560); and to the Arabidopsis Biological Resource Center for providing the T-DNA tagged lines of *A. thaliana*. This work was supported by a Specially Promoted Research of Grant-in-Aid for Scientific Research to I.H-N. (no. 22000014) and by a Grant-in-Aid for Scientific Research to K.T. (no. 20570036 and 25650096) from the Japan Society for the Promotion of Science (JSPS).

References

1. Starr, D.A., and Fridolfsson, H.N. (2010). Interactions between nuclei and the cytoskeleton are mediated by SUN-KASH nuclear-envelope bridges. Annu Rev Cell Dev Biol *26*, 421-444.
2. Metzger, T., Gache, V., Xu, M., Cadot, B., Folker, E.S., Richardson, B.E., Gomes, E.R., and Baylies, M.K. (2012). MAP and kinesin-dependent nuclear positioning is required for skeletal muscle function. Nature *484*, 120-124.
3. Chytilova, E., Macas, J., Sliwinska, E., Rafelski, S.M., Lambert, G.M., and Galbraith, D.W. (2000). Nuclear dynamics in *Arabidopsis thaliana*. Mol Biol Cell *11*, 2733-2741.
4. Tamura, K., Fukao, Y., Iwamoto, M., Haraguchi, T., and Hara-Nishimura, I. (2010). Identification and characterization of nuclear pore complex components in *Arabidopsis thaliana*. Plant Cell *22*, 4084-4097.
5. Graumann, K., Runions, J., and Evans, D.E. (2010). Characterization of SUN-domain proteins at the higher plant nuclear envelope. Plant J *61*, 134-144.
6. Murphy, S.P., Simmons, C.R., and Bass, H.W. (2010). Structure and expression of the maize (*Zea mays* L.) SUN-domain protein gene family: evidence for the existence of two divergent classes of SUN proteins in plants. BMC Plant Biol *10*, 269.
7. Oda, Y., and Fukuda, H. (2011). Dynamics of Arabidopsis SUN proteins during mitosis and involvement in nuclear shaping. Plant J *66*, 629-641.
8. Peremyslov, V.V., Mockler, T.C., Filichkin, S.A., Fox, S.E., Jaiswal, P., Makarova, K.S., Koonin, E.V., and Dolja, V.V. (2011). Expression, splicing, and evolution of the myosin gene family in plants. Plant Physiol *155*, 1191-1204.
9. Farquharson, K.L., and Staiger, C.J. (2010). Dissecting the functions of class XI myosins in moss and *Arabidopsis*. Plant Cell *22*, 1649.
10. Peremyslov, V.V., Prokhnevsky, A.I., and Dolja, V.V. (2010). Class XI myosins are required for development, cell expansion, and F-Actin organization in *Arabidopsis*. Plant Cell *22*, 1883-1897.
11. Shimmen, T., and Yokota, E. (2004). Cytoplasmic streaming in plants. Curr Opin Cell Biol *16*, 68-72.
12. Avisar, D., Abu-Abied, M., Belausov, E., Sadot, E., Hawes, C., and Sparkes, I.A. (2009). A comparative study of the involvement of 17 Arabidopsis myosin family members on the motility of Golgi and other organelles. Plant Physiol *150*, 700-709.
13. Ueda, H., Yokota, E., Kutsuna, N., Shimada, T., Tamura, K., Shimmen, T., Hasezawa, S., Dolja, V.V., and Hara-Nishimura, I. (2010). Myosin-dependent endoplasmic reticulum motility and F-actin organization in plant cells. Proc Natl Acad Sci USA *107*, 6894-6899.
14. Ojangu, E.L., Tanner, K., Pata, P., Jarve, K., Holweg, C.L., Truve, E., and Paves, H. (2012). Myosins XI-K, XI-1, and XI-2 are required for development of pavement cells, trichomes, and stigmatic papillae in Arabidopsis. BMC Plant Biol *12*, 81.
15. Zhao, Q., Brkljacic, J., and Meier, I. (2008). Two distinct interacting classes of nuclear envelope-associated coiled-coil proteins are required for the

tissue-specific nuclear envelope targeting of *Arabidopsis* RanGAP. Plant Cell *20*, 1639-1651.

16. Iwabuchi, K., Sakai, T., and Takagi, S. (2007). Blue light-dependent nuclear positioning in *Arabidopsis thaliana* leaf cells. Plant Cell Physiol *48*, 1291-1298.
17. Iwabuchi, K., Minamino, R., and Takagi, S. (2010). Actin reorganization underlies phototropin-dependent positioning of nuclei in *Arabidopsis* leaf cells. Plant Physiol *152*, 1309-1319.
18. Wilhelmsen, K., Ketema, M., Truong, H., and Sonnenberg, A. (2006). KASH-domain proteins in nuclear migration, anchorage and other processes. J Cell Sci *119*, 5021-5029.
19. Zhou, X., Graumann, K., Evans, D.E., and Meier, I. (2012). Novel plant SUN-KASH bridges are involved in RanGAP anchoring and nuclear shape determination. J Cell Biol *196*, 203-211.
20. Xu, X.M., Meulia, T., and Meier, I. (2007). Anchorage of plant RanGAP to the nuclear envelope involves novel nuclear-pore-associated proteins. Curr Biol *17*, 1157-1163.
21. Dupin, I., and Etienne-Manneville, S. (2011). Nuclear positioning: mechanisms and functions. Int J Biochem Cell Biol *43*, 1698-1707.
22. Lei, K., Zhang, X., Ding, X., Guo, X., Chen, M., Zhu, B., Xu, T., Zhuang, Y., Xu, R., and Han, M. (2009). SUN1 and SUN2 play critical but partially redundant roles in anchoring nuclei in skeletal muscle cells in mice. Proc Natl Acad Sci U S A *106*, 10207-10212.
23. Starr, D.A., and Han, M. (2002). Role of ANC-1 in tethering nuclei to the actin cytoskeleton. Science *298*, 406-409.
24. Gomes, E.R., Jani, S., and Gundersen, G.G. (2005). Nuclear movement regulated by Cdc42, MRCK, myosin, and actin flow establishes MTOC polarization in migrating cells. Cell *121*, 451-463.
25. Luxton, G.W., Gomes, E.R., Folker, E.S., Vintinner, E., and Gundersen, G.G. (2010). Linear arrays of nuclear envelope proteins harness retrograde actin flow for nuclear movement. Science *329*, 956-959.
26. Pollard, T.D., and Cooper, J.A. (2009). Actin, a central player in cell shape and movement. Science *326*, 1208-1212.
27. Woolner, S., and Bement, W.M. (2009). Unconventional myosins acting unconventionally. Trends Cell Biol *19*, 245-252.
28. Kapitein, L.C., and Hoogenraad, C.C. (2011). Which way to go? Cytoskeletal organization and polarized transport in neurons. Mol Cell Neurosci *46*, 9-20.
29. Higaki, T., Sano, T., and Hasezawa, S. (2007). Actin microfilament dynamics and actin side-binding proteins in plants. Curr Opin Plant Biol *10*, 549-556.
30. Tominaga, M., Kojima, H., Yokota, E., Orii, H., Nakamori, R., Katayama, E., Anson, M., Shimmen, T., and Oiwa, K. (2003). Higher plant myosin XI moves processively on actin with 35 nm steps at high velocity. EMBO J *22*, 1263-1272.

Figure legends

Figure 1. KAKU1/Myosin XI-i Localizes to the Nuclear Envelope and Is Required for Nuclear Shape and Movement.

(A and B) Nuclei of epidermal cells from 7-day-old wild-type (WT) (A) and *kaku1-1* (B) cotyledons were visualized by stable expression of Nup50a-GFP and the cell wall was counterstained with propidium iodide (magenta). Insets show the magnified images of nuclei.

(C and D) Nuclear envelopes in root hair cells of WT (C) and *kaku1-1* (D) were visualized by stable expression of SUN2-TagRFP and cell outlines are indicated.

(E and F) Electron micrographs of nuclear envelopes in mesophyll cells of WT (E) and *kaku1-1* (F) seedlings. Arrows indicate the irregularly and intricately invaginated nuclear envelope in *kaku1-1*. n, nucleus; c, chloroplast; v, vacuole.

(G) Schematic representation of the *myosin XI-i/KAKU1* gene (At4g33200) and the positions of the *kaku1-1* mutation and of each T-DNA insertion in three *kaku1* mutant alleles. Closed boxes, exons; solid lines, introns.

(H) RT-PCR of *myosin XI-i/KAKU1* and *Actin2* (*ACT2*) transcripts in WT and *kaku1* mutant alleles.

(I) Nuclei stained with Hoechst 33342 in root epidermal cells of *kaku1* mutant alleles. Numbers indicate nuclear circularity index (mean ± SD).

(J) Immunoblots of seedlings from WT and transgenic plants stably expressing YFP-*myosin XI-i/KAKU1* (YFP-XI-i-Δmotor) using anti-GFP and anti-BiP (loading control).

(K and L) Fluorescence images of epidermal cells from transgenic YFP-XI-i-Δmotor plants (K) and of a protoplast from tobacco cultured cells expressing GFP-myosin XI-i/KAKU1 full length (L). Arrows indicate the nuclear envelope.

(M) Movement of histone-GFP-labeled nuclei in root cells of WT, *kaku1-2*, and *kaku1-4* plants. Nuclei were imaged at 30 sec intervals for 45 min (see Movie S1 and Supplemental Experimental Procedure). Nuclei at 0, 22.5, and 45 min time points are

shown and the three images are merged.

Figure 2. Outer-nuclear Membrane Proteins WITs, which Interact with Myosin XI-i, Function in Anchoring Myosin XI-i to the Nuclear Membrane, and Regulate Nuclear Shape and Nuclear Movement.

(A) Immunoblots of the anti-GFP antibody pull-down products from transgenic plants expressing either free GFP or the YFP-XI-i-ΔmotoR.

(B) Subcellular localization of YFP-XI-i-ΔmotoR in hypocotyl and root cells of the wild-type (WT) and *wit1 wit2* plants. Arrows, nuclear envelope; arrowheads, plastid autofluorescence.

(C) Immunoblots of seedlings from WT plants, transgenic YFP-XI-i-ΔmotoR plants, and the *wit1 wit2* plants expressing YFP-XI-i-ΔmotoR using anti-GFP and anti-BiP (loading control).

(D) Nuclei stained with Hoechst 33342 in root epidermal cells of WT, *wit1*, *wit2*, and *wit1 wit2* plants.

(E) The circularity index of nuclei in root cells of WT, *wit1*, *wit2*, *wit1 wit2*, and *kaku1-4* plants. Mean ± standard deviation for $n > 90$ (Student's *t*-test, $*P < 0.0001$, $**P < 0.02$).

(F) Nuclear movement in root cells of WT and *wit1 wit2* plants. The images were captured and reconstituted as in the legend to Figure 1M (see Movie S1).

(G) Statistical quantification of nuclear movement displayed in Figure 1M and Figure 2F.

Figure 3. Myosin XI-i and WIT Are Required for the Dark-induced Nuclear Movement.

(A) Nuclear positioning in the mesophyll cells of the dark-adapted wild-type (WT), *kaku1-4*, and *wit1 wit2* leaves. Four sequential optical sections from the top (0 μm) to the bottom (15.1 μm) of mesophyll cells were imaged. Nuclei (histone-GFP, green),

cell walls (propidium iodide, magenta) and chloroplasts (autofluorescence, cyan) are shown. An arrowhead indicates nucleus at the center of the periclinal wall of the mesophyll cells in wild-type leaves and arrows indicate nuclei at the anticlinal wall in *kaku1-4* and *wit1 wit2*. See Supplementary Information (Movie S2) for three-dimensional images of the dark-adapted mesophyll cells showing nuclear positioning.

(B) Light- and dark-induced nuclear movement in the mesophyll cells of WT, *kaku1-2*, *kaku1-4,* and *wit1 wit2* leaves. Dark-adapted plants were irradiated with blue light for 3 h and then incubated in the dark for 16 h. The percentage of nuclei at the anticlinal wall was calculated. Data from five replicates represent mean ± standard deviation for $n > 200$ (Student's *t*-test, $*P < 0.01$).

Figure 4. A New Type of the Nucleocytoplasmic Linker of Plants and Its Comparison with Those of Animals

(A) Immunoblot showing the direct interactions between myosin XI-i and WIT. Recombinant GST-XI-i-Δmotor was incubated with one (x1) and 2.5-fold volumes (x2.5) of ProS2-WIT1. The pull-down products with GST-Sepharose were subjected to immunoblots with either anti-ProS2 or anti-GST antibody. The input:bound ratio is 1:8. Uncropped images of blots are shown in Figure S4.

(B) Immunoblot showing the interactions between myosin XI-i, WIT1, WIP1, and SUN2. Protein complexes in the tobacco leaves that transiently expressed both GFP- and RFP-tagged proteins were immunoprecipitated with anti-GFP antibody and then subjected to immunoblots with either anti-GFP or anti-RFP antibody. WIP1ΔVVPT is the unbound form to SUN proteins [19]. The input:IP (immunoprecipitates) ratio is 1:60. Uncropped images of blots are shown in Figure S4.

(C-E) Comparison of models of the nucleocytoplasmic linkers of plants and animals.

(C) Proposed model of a new type of nucleocytoplasmic linker that regulates the movement and shape of plant nuclei. The linker consists of myosin XI-i that binds to both the actin cytoskeleton and the outer-nuclear membrane WIT proteins. WIT

proteins interact with the SUN-WIP bridge.

(D) Model of animal nucleocytoplasmic linker that regulates nuclear movement and shape. The linker consists of motor proteins (kinesins and dyneins) that bind to both the microtubule cytoskeleton and the SUN-KASH bridge [1, 18].

(E) Model of the direct interaction between the actin cytoskeleton and the SUN-KASH bridge in animals that regulates nuclear anchoring and shape [22, 23].

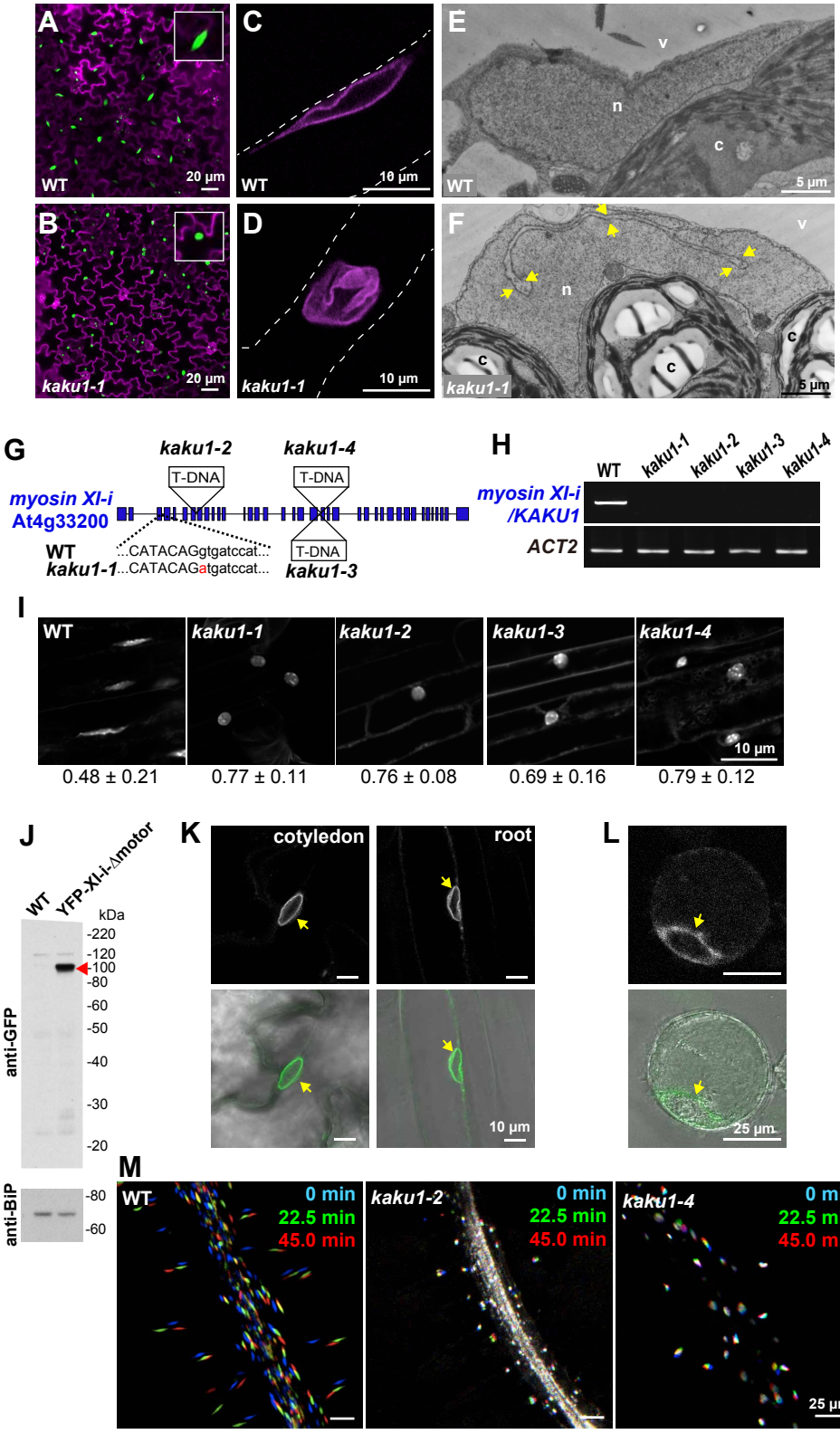
A
WT
20 μm
B
kaku1-1
20 μm
C
WT
10 μm
D
kaku1-1
10 μm
E
v
n
c
WT
5 μm
F
v
n
c
c
c
kaku1-1
5 μm
G
kaku1-2
kaku1-4
T-DNA
T-DNA
myosin XI-i
At4g33200
T-DNA
WT
...CATACAGgtgatccat...
kaku1-1
...CATACAGatgatccat...
kaku1-3
H
WT
kaku1-1
kaku1-2
kaku1-3
kaku1-4
myosin XI-i
/KAKU1
ACT2
I
WT
kaku1-1
kaku1-2
kaku1-3
kaku1-4
10 μm
0.48 ± 0.21
0.77 ± 0.11
0.76 ± 0.08
0.69 ± 0.16
0.79 ± 0.12
J
WT
YFP-XI-i-Δmotor
kDa
-220
-120
-100
-80
-60
-50
-40
-30
-20
anti-GFP
anti-BiP
-80
-60
K
cotyledon
root
10 μm
L
25 μm
M
WT
0 min
22.5 min
45.0 min
kaku1-2
0 min
22.5 min
45.0 min
kaku1-4
0 min
22.5 min
45.0 min
25 μm

Figure 1

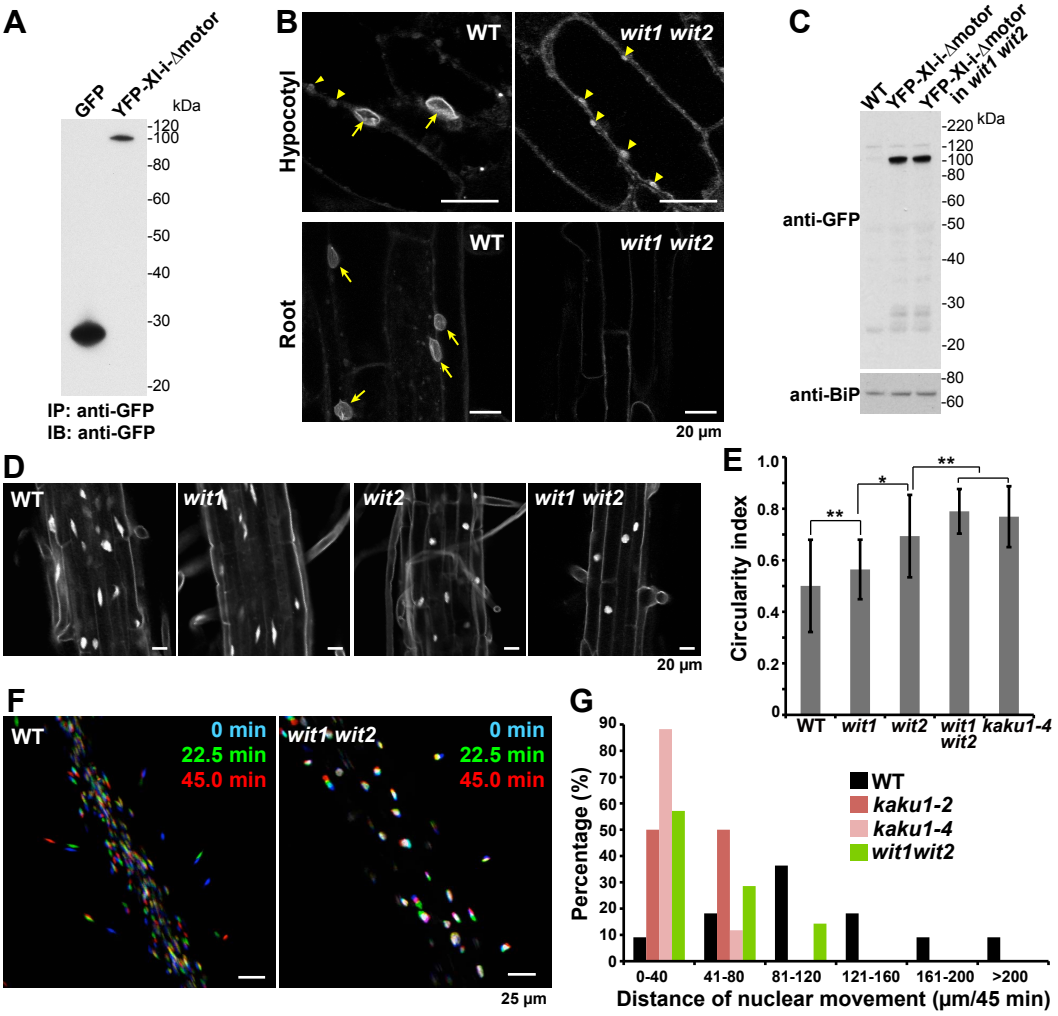
A
GFP
YFP-Xl-i-Δmotor
kDa
120
100
80
60
50
40
30
20
IP: anti-GFP
IB: anti-GFP
B
WT
wit1 wit2
Hypocotyl
Root
20 μm
C
WT
YFP-Xl-i-Δmotor
YFP-Xl-i-Δmotor in wit1 wit2
kDa
220
120
100
80
60
50
40
30
20
anti-GFP
anti-BiP
D
WT
wit1
wit2
wit1 wit2
20 μm
E
Circularity index
1.0
0.8
0.6
0.4
0.2
0
**
*
**
WT
wit1
wit2
wit1 wit2
kaku1-4
F
WT
wit1 wit2
0 min
22.5 min
45.0 min
25 μm
G
Percentage (%)
90
80
70
60
50
40
30
20
10
0
WT
kaku1-2
kaku1-4
wit1wit2
0-40
41-80
81-120
121-160
161-200
>200
Distance of nuclear movement (μm/45 min)

Figure 2

Figure 3

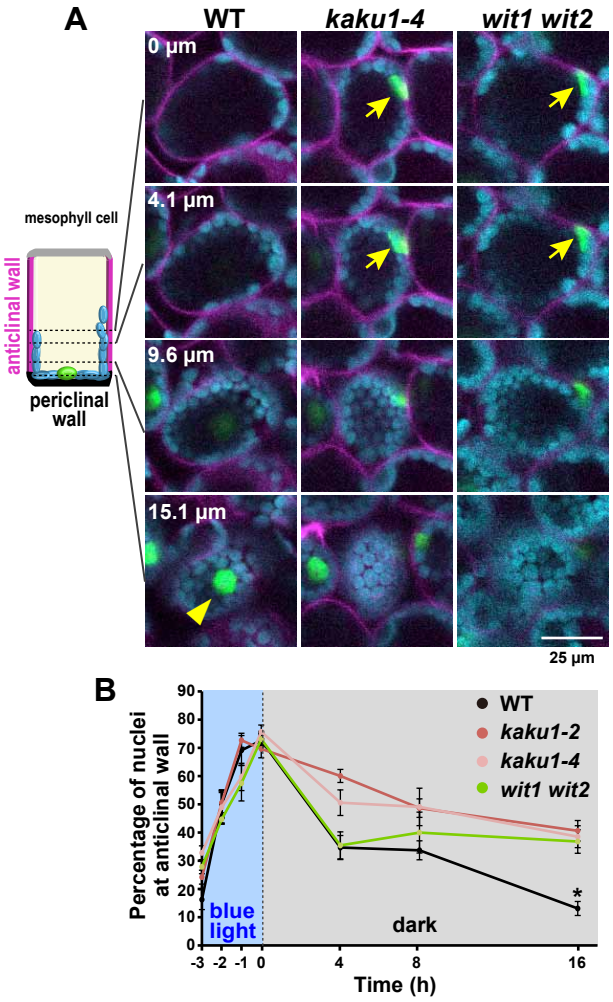

Figure 3

Figure 4

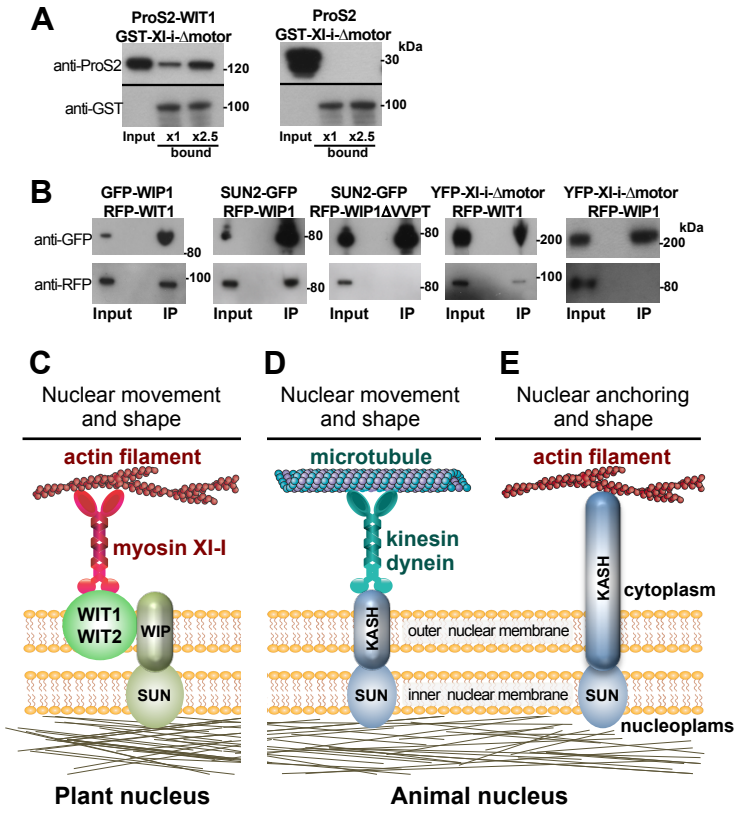

Figure 4

Supplemental Information

Myosin XI-i Links the Nuclear Membrane with the Cytoskeleton for Nuclear Movement and Shape in *Arabidopsis thaliana*

Kentaro Tamura, Kosei Iwabuchi, Yoichiro Fukao, Maki Kondo, Keishi Okamoto, Haruko Ueda, Mikio Nishimura, and Ikuko Hara-Nishimura

Supplemental Inventory

Figure S1. Irregularly and Intricately Invaginated Nuclear Envelope in Different Tissues of the *A. thaliana* Mutant *kaku1-1.*

Figure S2. Endoplasmic Reticulum Architecture in Petiole Epidermal Cells and Cortical Actin Filaments in Hypocotyl Epidermal Cells from Wild-Type, *kaku1-4,* and *xi2-2 xik-2* Mutant Plants.

Figure S3. WITs Are Required for Anchoring Myosin XI-i to the Nuclear Membrane.

Figure S4. Full scans of Original Blots for Data in Figure 4.

Supplemental Experimental Procedures

Supplemental References

Supplemental Movie S1. Nuclear Movement in Root Cells of Wild-Type (WT), *kaku1-2,* and *wit1 wit2* Plants.

Supplemental Movie S2. Three-Dimensional Images of the Dark-Adapted Mesophyll Cells Showing Nuclear Positioning in the Wild-Type (WT), *kaku1-4*, and *wit1 wit2* Leaves.

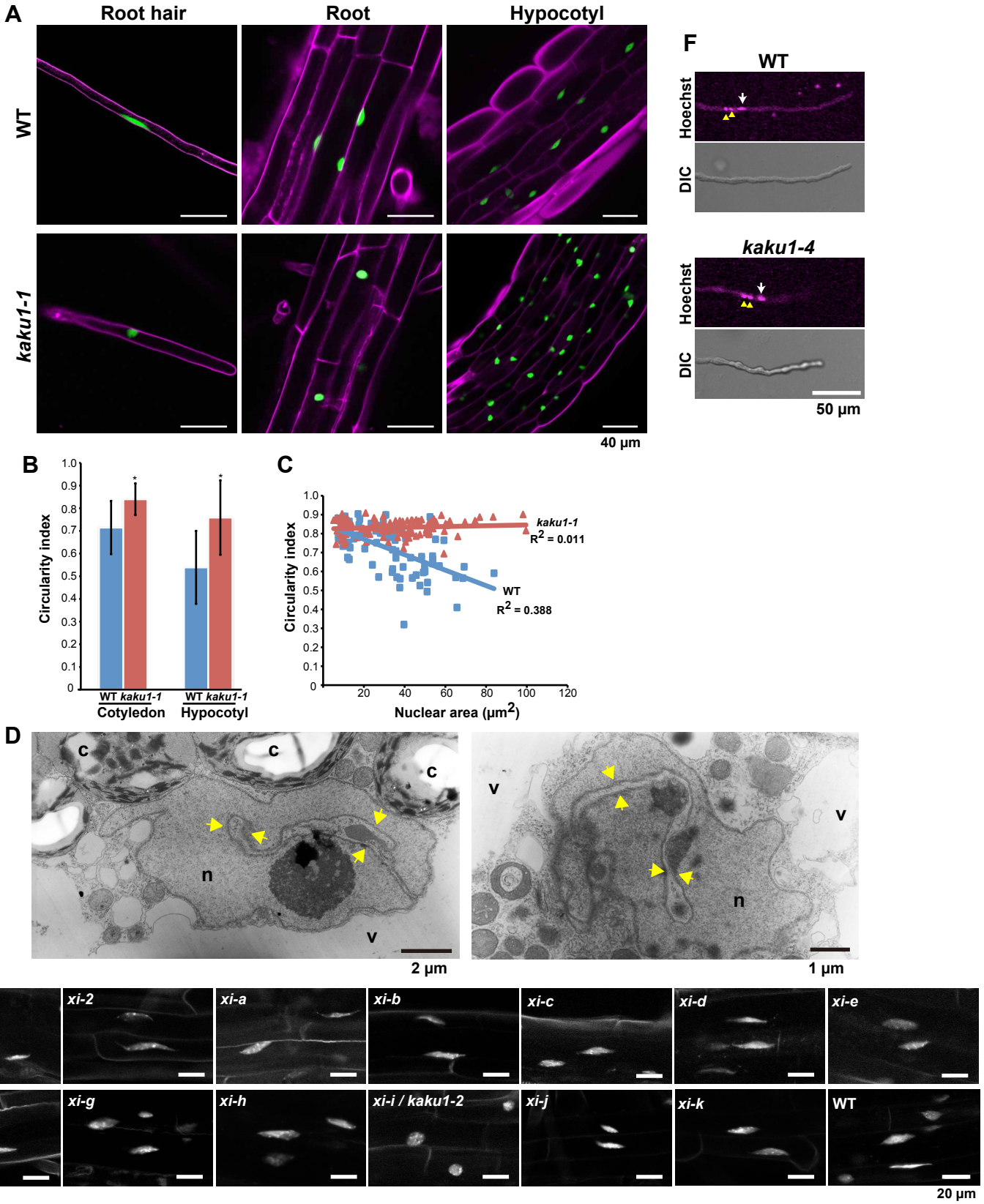

Figure S1. Irregularly and Intricately Invaginated Nuclear Envelope in Different Tissues of the *A. thaliana* Mutant *kaku1-1*.
(A) Fluorescence images of epidermal cells from 7-day-old seedlings of wild-type (WT) and *kaku1-1*. Nuclei were visualized by stable expression of nucleus-localized GFP (Nup50a-GFP, green). The cell wall was counterstained with propidium iodide (magenta).
(B) Statistical analysis of nuclear shape in cotyledons and hypocotyls of wild-type (WT) and *kaku1-1*. Nuclei stained with Hoechst 33342 were analyzed with ImageJ to calculate the nuclear circularity index. Data represent the mean ± standard deviation for n > 90 (Student' s *t*-test, *p < 0.001).
(C) Scatter plot analysis of circularity index (ordinate) versus nuclear projection area (abscissa) of wild-type (WT) and *kaku1-1* mutant cotyledons. The solid lines show linear regressions.
(D) Ultrastructure of nuclei in leaf epidermal cells of *kaku1-1* mutants. Arrows indicate deeply invaginated nuclear envelope. n, nucleus; c, chloroplast; v, vacuole.
(E) Nuclear shape of a single mutant line defective in each member of the *A. thaliana* myosin XI family. Representative nuclei stained with Hoechst 33342 of epidermal cells of cotyledons are shown. *A. thaliana* has 13 members of myosin XI family; myosins XI-a to XI-k and myosins XI-1 and XI-2 (formally denoted as Mya1 and Mya2, respectively).
(F) Vegetative nuclei (arrows) and generative nuclei (arrowheads) in pollen tubes of wild type (WT) and *kaku1-4* were stained with Hoechst 33342.

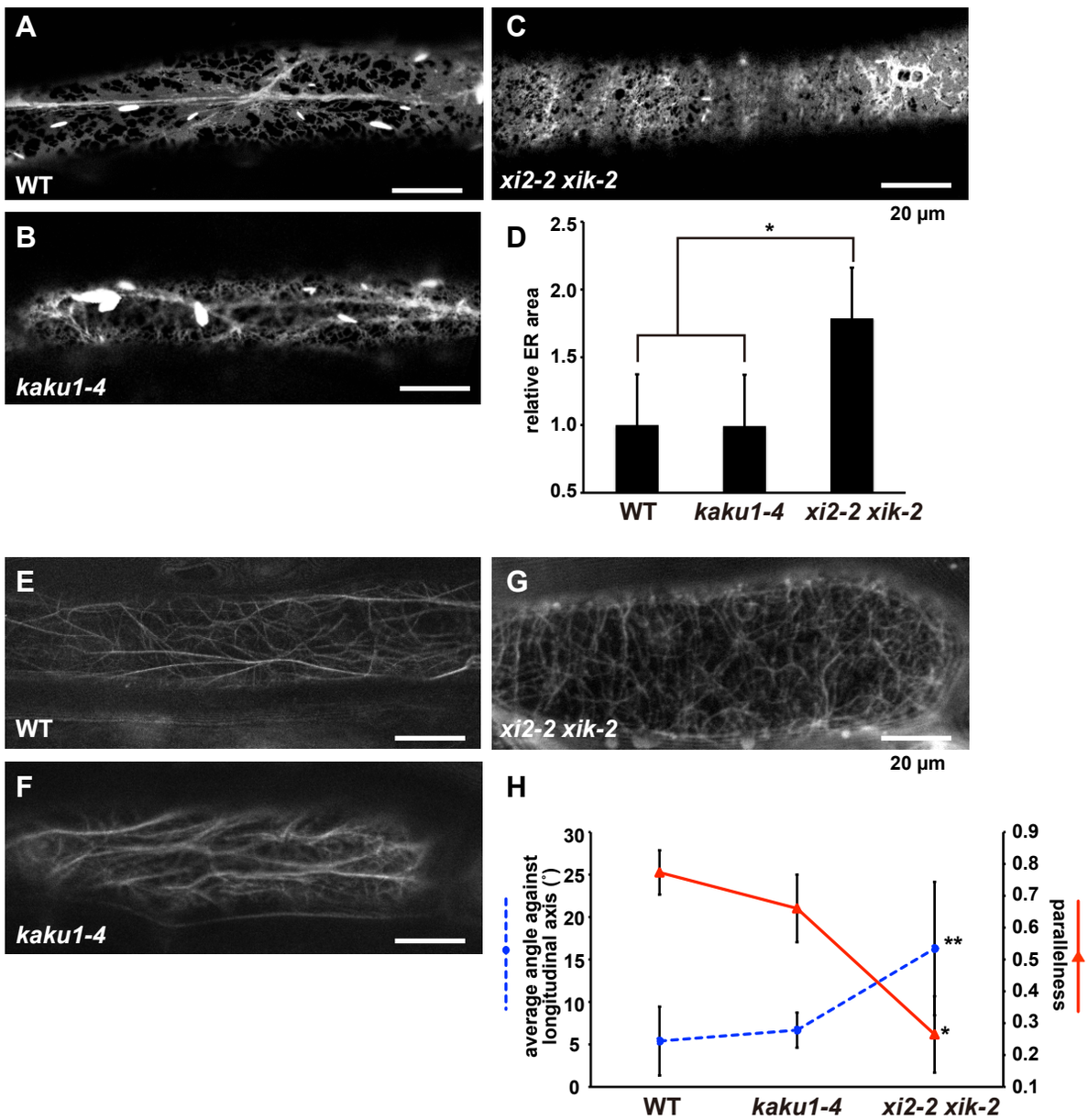

Figure S2. Endoplasmic Reticulum Architecture in Petiole Epidermal Cells and Cortical Actin Filaments in Hypocotyl Epidermal Cells from Wild-Type, *kaku1-4*, and *xi2-2 xik-2* Mutant Plants.
(A-C) Fluorescence images of endoplasmic reticulum (ER) visualized by stable expression of SP-GFP-HDEL in petiole epidermal cells of wild-type (WT) (A), *kaku1-4* (B), and *xi2-2- xik-2* (C).
(D) Quantification of relative ER area in petiole cells of wild-type (WT), *kaku1-4*, and *xi2-2- xik-2*. Data represent the mean ± standard deviation for n > 10 (Student' s *t*-test, *p < 0.001).
(E-G) Fluorescence images of cortical acitin filaments visualized by stable expression of tdTomato-ABD2 in hypocotyl epidermal cells of wild-type (WT) (E), *kaku1-4* (F), and *xi2-2- xik-2* (G).
(H) Orientation of actin filament bundles was evaluated by two indices: Average angle of actin filament bundles against a longitudinal axis and parallelness. Data represent the mean ± standard deviation for n > 10 (Student' s t-test, *p < 0.001, **p < 0.05).

A

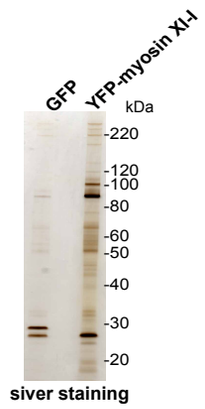

B

AGI code	Annotation	Score
AT4G33200.1	XI-I (Myosin-like protein XI-I); motor/ protein binding	306
ATCG00480.1	chloroplast-encoded gene for beta subunit of ATP synthase	187
AT2G27730.1	Identical to Uncharacterized mitochondrial protein	121
AT2G28900.1	OEP16 (OUTER ENVELOPE PROTEIN 16)	55
AT4G02770.1	PSAD-1 (photosystem I subunit D-1)	51
AT3G45570.1	zinc finger (C3HC4-type RING finger) family protein	48
AT2G44410.1	protein binding / zinc ion binding	47
AT1G59870.1	PDR8/PEN3 (PLEIOTROPIC DRUG RESISTANCE8)	46
AT5G20490.1	XIK (Myosin-like protein XIK	45
AT1G17580.1	MYA1 (ARABIDOPSIS MYOSIN)	42
AT2G18960.1	AHA1 (ARABIDOPSIS H+ ATPASE 1)	41
AT5G43970.1	TOM22-V	40
AT2G37620.1	ACT1 (ACTIN 1); structural constituent of cytoskeleton	39
AT2G42100.1	actin, putative	39
AT1G80660.1	AHA9 (Arabidopsis H(+)-ATPase 9)	32
AT5G13490.1	AAC2 (ADP/ATP CARRIER 2)	32
AT5G13950.1	similar to unknown protein	32
AT5G40420.1	OLEO2 (OLEOSIN 2)	32
AT1G03160.1	FZL (FZO-LIKE)	31
AT1G68910.1	WIT2	29
AT5G57110.1	ACA8 (AUTOINHIBITED CA2+ -ATPASE, ISOFORM 8)	28
AT1G09760.1	U2A' (U2 small nuclear ribonucleoprotein A)	27
AT4G14385.1	similar to unnamed protein product	27
AT3G57330.1	ACA11 (AUTOINHIBITED CA2+-ATPASE 11)	26
AT4G00355.1	similar to unknown protein	26
AT5G05170.1	CESA3 (CELLULOSE SYNTHASE 3)	26
AT2G24520.1	AHA5 (ARABIDOPSIS H(+)-ATPASE 5)	25
AT4G30190.1	AHA2 (Arabidopsis H(+)-ATPase 2)	25
AT5G12100.1	pentatricopeptide (PPR) repeat-containing protein	25
AT5G22750.1	RAD5	25
AT5G49310.1	importin alpha-1 subunit, putative	25
AT5G62670.1	AHA11 (ARABIDOPSIS H(+)-ATPASE 11)	25
AT1G63020.1	NRPD1a (NUCLEAR RNA POLYMERASE D 1A)	24
AT3G27870.1	haloacid dehalogenase-like hydrolase family protein	24
AT3G51770.1	ETO1 (ETHYLENE OVERPRODUCER 1)	24
AT4G27690.1	vacuolar protein sorting-associated protein 26, putative	24
AT1G03370.1	C2 domain-containing protein	23
AT1G33170.1	dehydration-responsive family protein	23
AT2G21390.1	coatomer protein complex, subunit alpha, putative	23
AT3G49900.1	BTB/POZ domain-containing protein	23
AT4G34500.1	protein kinase family protein	23
AT5G10170.1	inositol-3-phosphate synthase, putative	23
AT3G44530.1	HIRA	22
AT5G08660.1	similar to unknown protein	22

C

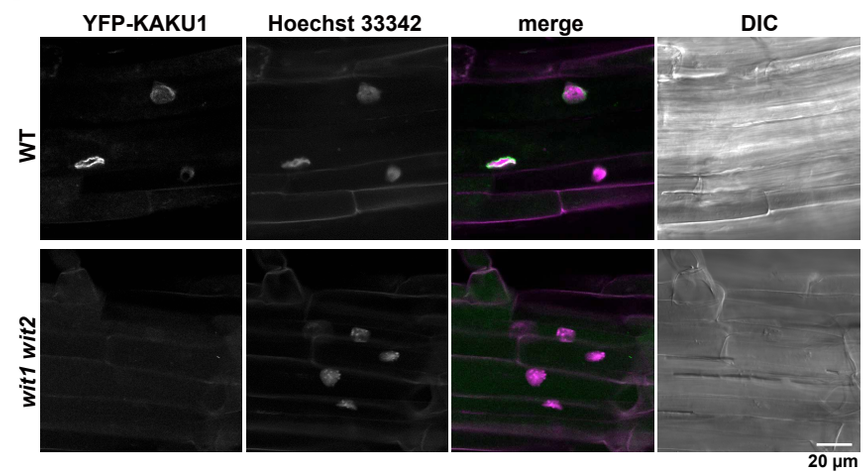

Figure S3. WITs Are Required for Anchoring Myosin XI-i to the Nuclear Membrane.
(A) Silver staining of the anti-GFP antibody pull-down products from transgenic plants expressing either free GFP or the YFP-myosin XI-i.
(B) LTQ-Orbitrap mass spectrometry identified the listed 44 proteins specifically in transgenic YFP-myosin XI-i plants, but not in the transgenic free-GFP plants. The Arabidopsis Genome Initiative (AGI) codes and annotations were obtained from the TAIR database (http://www.arabidopsis.org).
(C) Images showing subcellular localization of YFP-myosin XI-i in the root epidermal cells from wild-type (WT) and *wit1 wit2* plants. Nuclei are stained with Hoechst 33342. The merged images are also shown.

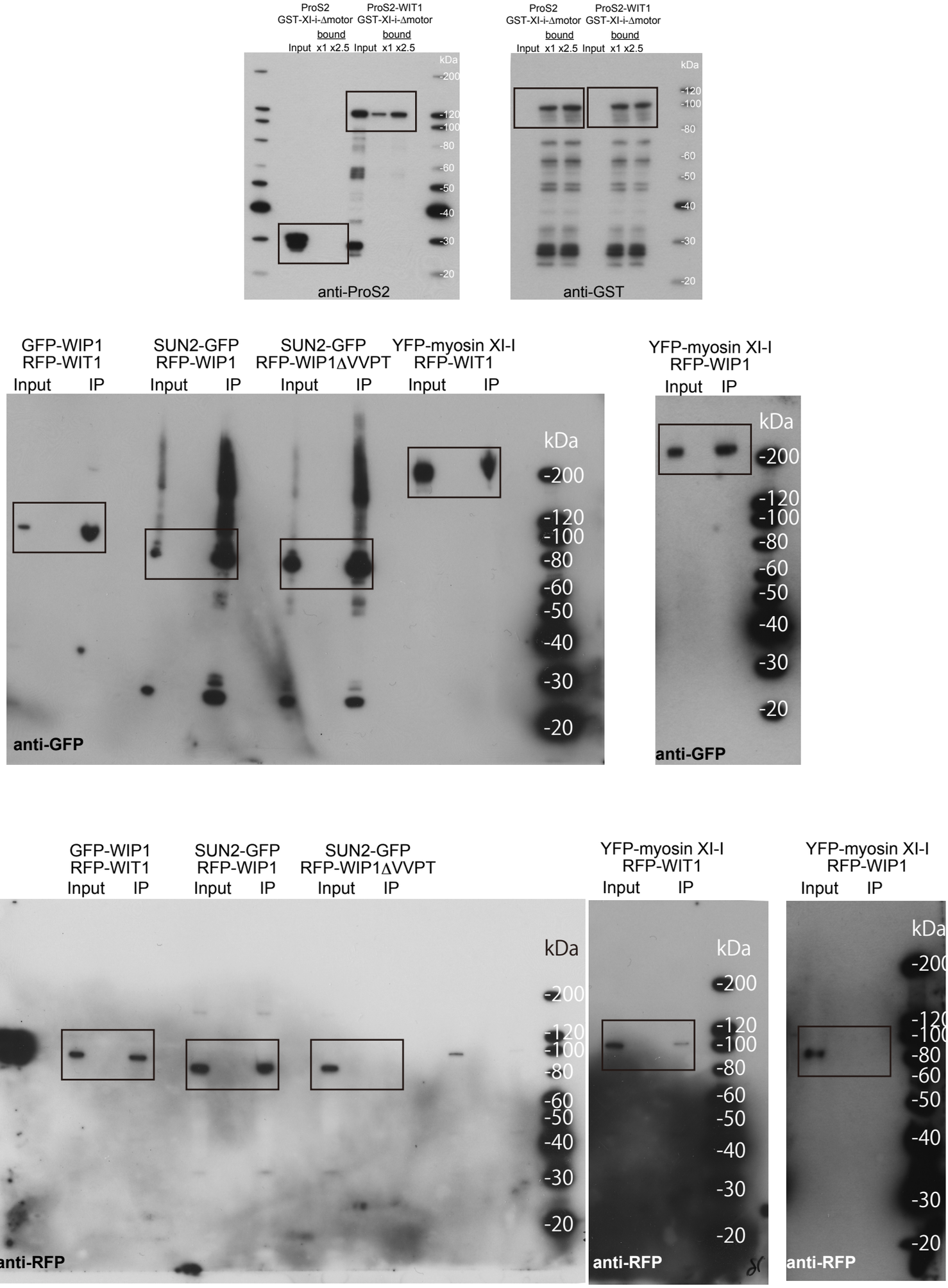

Figure S4. Full Scans of Oiginal Blots for Data in Figure 4.

Supplemental Experimental Procedures

Plant Materials

Wild-type of *Arabidopsis thaliana* (ecotype Columbia) plants and the transgenic *A. thaliana* plant that expresses Nup50a-GFP were used. The T-DNA insertion mutants, SAIL_1271_E11 (*kaku1-2*), SALK_092026 (*kaku1-3*), SALK_082443 (*kaku1-4*), SALK_022140C (*xi-1)*, SALK_127984 (*xi-2*), SALK_086989 (*xi-a*), SALK_016579 (*xi-b*), SALK_097302 (*xi-c*), SALK_082078 (*xi-d*), SALK_122989 (*xi-e*), SALK_094787 (*xi-f*), SALK_018032 (*xi-g*), SALK_014709 (*xi-h*), SALK_063159 (*xi-j*), and SALK_067972 (*xi-k*) were obtained from the Arabidopsis Biological Resource Center at Ohio State University. Seeds of *wit1-1*, *wit2-1*, and *wit1-1 wit2-1* mutants were kindly provided by Iris Meier (Ohio State University, USA).

Isolation of the *kaku1-1* Mutant and a Map-based Cloning of the *KAKU1* Gene

Nup50a-GFP seeds were mutagenized by methanesulfonic acid ethyl ester treatment. M_2 seeds were collected from individual M_1 plants to generate M_2 lines. Each seedling was examined with a fluorescence microscope, and a mutant line that exhibited disorganized nuclear structure was selected. Map-based cloning was performed as described previously [1].

Stable Expression of Fluorescent Protein Fusions in *A. thaliana*

Genomic DNA of histone H2A (At2g38810) and cDNA of AtSUN2 (At3g10730) fragments were generated using specific primers (histone H2A; 5’-CACCATGGCTGGTAAAGGTGGGAAAGG-3’ and 5’-ATCCTTGGTGACTTTGTTGACAAG-3’, AtSUN2; 5’-CACCATGTCGGCGTCAACGGTGTCAATCA-3’ and 5’-AGCATGAGCAACAGAGACTGAGTC-3’) and cloned into the pENTR/D-TOPO vector (Invitrogen, USA). To generate the DNA constructs for fluorescent protein fusions, each of the cloned DNA fragment was transferred from the entry clone to either the pGWB405 Gateway destination vector (for GFP constructs) or the pGWB560 (for TagRFP constructs) [2, 3] by an *in-vitro* recombination *att*L x *att*R reaction. GFP-tagged histone H2B (At5g22880) was used as a nuclear marker. We also generated transgenic plants expressing the YFP-myosin XI-i, by using myosin XI-i lacking the motor domain, as reported previously. The YFP-myosin XI-i construct was kindly provided by Maureen Hanson (Cornell University, USA) [4]. Transgenic plants expressing either ER-localized GFP or tdTomato-ABD2 were generated

previously [5].

RT-PCR Analysis

Total RNA was isolated from 10-day-old seedlings using the RNeasy Plant Mini Kit (Qiagen, USA). Reverse transcription was performed using Ready-To-Go RT-PCR Beads (GE Healthcare) with an oligo $(dT)_{12-18}$ primer. DNA fragments were generated using specific primers (ACT2; 5'-AGAGATTCAGATGCCCAGAAGTCTTGTTCC-3' and 5'-GAGTATGATGAGGCAGGTCCAGGAATCGTT-3' and myosin XI-i; 5'-ATGAGAAATTGTCTTCCAATGG-3' and 5'-TCAAATGATCTGCTTTGAGGTT-3'). *ACT2* was amplified in 26 and *myosin XI-i* in 35 PCR cycles, respectively. PCR products were visualized with ethidium bromide. Quantitative RT-PCR was performed with specific primers (myosin XI-i; 5'- CTCGCCTACGCGAAAATCAT- 3' and 5'-TGTGCAACATTCACGACGAA- 3' and NDUFA8; 5'-CTGCGTGCTTGGCTTGCTG- 3' and 5'-GGCTTCTTGCTCTTTCCTACACA- 3') and SYBR Premix Ex Taq II (Takara).

Confocal Laser Scanning Microscopy and Electron Microscopy

Confocal images were obtained using a laser scanning microscopes (Zeiss LSM 780 and Zeiss LSM 510 META; Carl Zeiss) equipped with a 405 nm blue diode laser, 488 nm 40-mW Ar/Kr laser, or a 544 nm 1 mW He/Ne laser, and a 100 x 1.45 N.A. oil immersion objective (alpha Plan-Fluar, 000000-1084-514, Carl Zeiss), 63 x 1.2 N.A. water immersion objective (C-Apochromat, 441777-9970-000, Carl Zeiss), or 40 x 0.95 N.A. dry objective (Plan-Apochromat, 440654-9902-000, Carl Zeiss). Image analysis was performed using either LSM image examiner software (Carl Zeiss) or ImageJ 1.45s software (NIH, USA). Transmission electron microscopy was essentially performed as described previously [1].

SDS-PAGE and Immunoblot Analysis

Protein extracts from seedlings and isolated nuclei were subjected to SDS-PAGE followed by either Coomassie blue staining or immunoblot analysis. Immunoreactive signals were detected with the ECL detection system (GE Healthcare), using anti-GFP antibody (JL-8, Clontech) at 1:1,000 dilution, or anti-BiP antibody at 1:10,000 dilution [6].

Coimmunoprecipitation Experiments

Genomic DNA of WIP1 (At4g26455) and WIT1 (At5g11390) fragments were generated using specific primers (WIP1; 5'-AACCAATTCAGTCGACATGGATTTGGAGAGTGAAAGCTC-3' and 5'-

AAGCTGGGTCTAGATATCCTCATGTGGGTACAACAGTATC-3', WIT1; 5'-AACCAATTCAGTCGACATGGAAACAGAAACGGAACATG-3' and 5'-AAGCTGGGTCTAGATATCCTTACATGTTTTGCTGGGATATA-3') and cloned into the pENTR1A vector (Invitrogen, USA). To generate the fluorescent protein fusions, each of the cloned DNA fragment was transferred from the entry clone to either the pGWB406 Gateway destination vector (for GFP constructs) or the pGWB461 (for TagRFP constructs) [2, 3] by an *in-vitro* recombination *att*L x *att*R reaction. Fluorescent proteins were co-expressed transiently in *N. tabacum* leaves by *Agrobacterium* infiltration. Immunoprecipitation was performed with μMACS Epitope Tag Protein Isolation Kits (Miltenyi Biotec, Gladbach, Germany) as follows. The leaves (0.5 - 2.0 g) were homogenized in 1.5 to 6.0 ml of lysis buffer (50 mM Tris-HCl, pH 8.0, 150 mM NaCl, 1% Triton X-100, and protease inhibitors cocktail) and then centrifuged at 15,000 rpm for 10 min to obtain a soluble lysate. Antibody-conjugated beads (50 μl) were added to the lysate and then the protein complexes were purified according to a manufacturers' instruction. The immunoprecipitates were then analyzed by immunoblot analysis with anti-GFP antibody at 1:1,000 or anti-RFP antibody (Invitrogen) at 1:500.

Immunoprecipitation and Mass Spectrometry

Immunoprecipitation was performed with μMACS Epitope Tag Protein Isolation Kits (Miltenyi Biotec) as described above. The protein components of the immunoprecipitates were briefly separated on a 2 cm long SDS gel. Gel slices isolated from each lane were cut into a <50 kDa fraction, a 50-100 kDa fraction, and a >100 kDa fraction. Each excised gel fraction was subjected to trypsin digestion. The extracted peptides were combined and then evaporated to 10 μl in a vacuum concentrator. LC-MS/MS analyses were performed using the LTQ-Orbitrap XL-HTC-PAL system (Thermo Fisher Scientific, Bremen, Germany), as described previously. The Mascot search parameters were set as follows: threshold of the ion-score cut-off, 0.05; peptide tolerance, 10 ppm; MS/MS tolerance, ±0.8 Da; and peptide charge, 2+ or 3+. The search was also set to allow one missed cleavage by trypsin, a carboxymethylation modification of cysteine residues, and a variable oxidation modification of methionine residues.

Pull-Down Assay

Glutathione-S-transferase-XI-i-Δmotor (GST-XI-i-Δmotor), 6x His-ProS2, and 6x His-ProS2-WIT1 were expressed in *Escherichia coli* BL21 (DE3) (Novagen). According to the manufacturers' instructions, the recombinant protein

GST-XI-i-Δmotor was purified and bound to glutathione–Sepharose 4B (GE Healthcare). The 6x His-ProS2 fusion proteins were purified on TALON metal affinity resin (Takara). The purified 6x His-ProS2 fusions were incubated with GST-XI-i-Δmotor-trapped Sepharose beads in a buffer (50 mM HEPES, pH 7.4, 150 mM NaCl, 1 mM $MgCl_2$, 1 mM DTT, and protease inhibitors cocktail) for 1 h. After washing the beads with the buffer, bound proteins were eluted with 2x SDS-sample buffer and then subjected to immunoblot analysis.

Nuclear Movement Assay

Light-dependent nuclear relocation was performed as described previously [7]. For quantification of nuclear movement in root cells, transgenic plants expressing GFP-tagged histone were grown on glass bottom dishes. Two-week-old seedlings were used for the quantification of nuclear movement. All time-lapse series were taken as a set of z-stacks over time (four-dimensional imaging) with eight series of optical sections every 6 μm. The individual z-stacks were collected every 30 s over a period of 45 min. At every time point the 3D optical sections were reduced to 2D maximal projection images and transformed to a 2D time-lapse movie. The image analysis was performed with ImageJ software.

Hoechst Staining

Nuclei were stained for 30 min with 1 μg/ml Hoechst 33342 solution, 3.7% (w/v) paraformaldehyde, 10% (v/v) DMSO, 3% (v/v) NP-40, 50 mM PIPES-KOH (pH 7.0), 1 mM $MgSO_4$, and 5 mM EGTA. The stained nuclei were inspected with a confocal laser scanning microscope by exciting with a 405-nm diode laser (Carl Zeiss).

Quantification of Endoplasmic Reticulum (ER) area and Actin Filament Organization

ER areas were measured from threshold images in ROI (7.02 x 7.02 μm^2) with ImageJ software. Quantification of actin organization was performed as described previously [8].

Statistics

Mean, S.D., and two-tailed Student's *t*–test calculations were performed using Microsoft Excel with StatPlus software.

Supplemental References

1. Tamura, K., Shimada, T., Kondo, M., Nishimura, M., and Hara-Nishimura, I. (2005). KATAMARI1/MURUS3 Is a novel golgi membrane protein that is required for endomembrane organization in Arabidopsis. Plant Cell *17*, 1764-1776.
2. Nakagawa, T., Suzuki, T., Murata, S., Nakamura, S., Hino, T., Maeo, K., Tabata, R., Kawai, T., Tanaka, K., Niwa, Y., et al. (2007). Improved Gateway binary vectors: high-performance vectors for creation of fusion constructs in transgenic analysis of plants. Biosci Biotechnol Biochem *71*, 2095-2100.
3. Nakamura, S., Mano, S., Tanaka, Y., Ohnishi, M., Nakamori, C., Araki, M., Niwa, T., Nishimura, M., Kaminaka, H., Nakagawa, T., et al. (2010). Gateway binary vectors with the bialaphos resistance gene, bar, as a selection marker for plant transformation. Biosci Biotechnol Biochem *74*, 1315-1319.
4. Reisen, D., and Hanson, M.R. (2007). Association of six YFP-myosin XI-tail fusions with mobile plant cell organelles. BMC Plant Biol *7*, 6.
5. Nakano, R.T., Matsushima, R., Ueda, H., Tamura, K., Shimada, T., Li, L., Hayashi, Y., Kondo, M., Nishimura, M., and Hara-Nishimura, I. (2009). GNOM-LIKE1/ERMO1 and SEC24a/ERMO2 are required for maintenance of endoplasmic reticulum morphology in *Arabidopsis thaliana*. Plant Cell *21*, 3672-3685.
6. Hatano, K., Shimada, T., Hiraiwa, N., Nishimura, M., and Hara-Nishimura, I. (1997). A rapid increase in the level of binding protein (BiP) is accompanied by synthesis and degradation of storage proteins in pumpkin cotyledons. Plant Cell Physiol *38*, 344-351.
7. Iwabuchi, K., Sakai, T., and Takagi, S. (2007). Blue light-dependent nuclear positioning in *Arabidopsis thaliana* leaf cells. Plant Cell Physiol *48*, 1291-1298.
8. Ueda, H., Yokota, E., Kutsuna, N., Shimada, T., Tamura, K., Shimmen, T., Hasezawa, S., Dolja, VV., and Hara-Nishimura, I. (2010). Myosin-dependent endoplasmic reticulum motility and F-actin organization in plant cells. Proc Natl Acad Sci USA *107*, 6894-6899.

Supplemental Movie S1. Nuclear Movement in Root Cells of Wild-Type (WT), *kaku1-2,* and *wit1 wit2* Plants.

Nuclei visualized with histone-GFP were imaged with a confocal laser scanning microscope. Projections were reconstituted from 6 sequential images taken along the optical z-axis (6.5 μm intervals), and from 90 time-sequential images captured at 30 sec intervals for 45 min. Scale bar represents 25 μm.

Supplemental Movie S2. Three-Dimensional Images of the Dark-Adapted Mesophyll Cells Showing Nuclear Positioning in the Wild-Type (WT), *kaku1-4*, and *wit1 wit2* Leaves.

Sequential optical sections from top to bottom of mesophyll cells were imaged with a confocal laser scanning microscope. The images were reconstituted as a projection movie. Nuclei (histone-GFP, green), cell walls (propidium iodide, magenta) and chloroplasts (autofluorescence, cyan) are shown.